Materials & Design 213 (2022) 110354

Contents lists available at ScienceDirect

Materials & Design

journal homepage: www.elsevier.com/locate/matdes

# Functionalized carbon nanotube-encapsulated magnesium-based nanocomposites with outstanding mechanical and biological properties as load-bearing bone implants

Somayeh Abazari [a], Ali Shamsipur [a], Hamid Reza Bakhsheshi-Rad [b,*], Filippo Berto [c,*]

[a] Department of Materials and Metallurgical Engineering, Amirkabir University of Technology, Tehran, Iran
[b] Advanced Materials Research Center, Department of Materials Engineering, Najafabad Branch, Islamic Azad University, Najafabad, Iran
[c] Department of Mechanical and Industrial Engineering, Norwegian University of Science and Technology, 7491 Trondheim, Norway

## HIGHLIGHTS

- Mg-based nanocomposite containing fCNTs were prepared by semi-powder metallurgy, sintering, and extrusion process.
- Crack tip shielding effect, crack bridging and crack deflection were determined as crucial toughening mechanisms in Mg/fCNTs composites.
- Composite with the lowest fCNTs concentration has the best corrosion resistance.
- SBF immersion and cell culture experiments demonstrated Mg/fCNTs nanocomposite has appropriate bioactivity and biocompatibility for the use as biomaterials.
- Mg-3Zn/0.4fCNT composite presented outstanding mechanical properties and biological properties.

## GRAPHICAL ABSTRACT

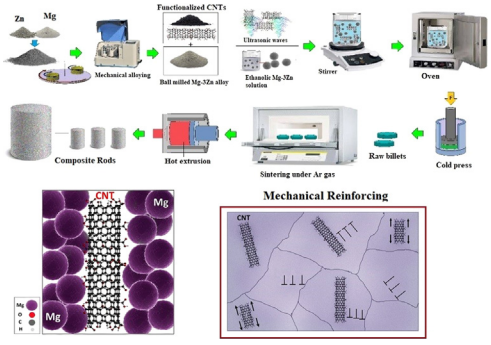


## ARTICLE INFO

*Article history:*
Received 7 August 2021
Revised 2 November 2021
Accepted 21 December 2021
Available online 23 December 2021

*Keywords:*
Nanocomposites
Magnesium
Carbon nanotubes
Mechanical properties
Biocompatibility

## ABSTRACT

Magnesium (Mg)-based composites have recently been studied as biodegradable material for the fabrication of orthopedic implants. Nevertheless, in physiological environments, proper mechanical properties and sufficient degradation rate are needed. In this paper, zinc (Zn) was uniformly distributed in the magnesium matrix using a ball milling process, and then the composite of Mg-3Zn/xfCNTs (x = 0, 0.2, 0.4, and 0.8 wt%) was successfully fabricated using a combination of semi-powder metallurgy, sintering and extrusion processes for use as a biodegradable load-bearing implant. The influence of functionalized carbon nanotubes (fCNTs) content on compressive strength, corrosion behavior and in vitro bioactivity (apatite formation ability and cytocompatibility) of the composite was investigated. The key toughening mechanisms that resist crack propagation include fCNTs pull-out, grain bridging by fCNTs, Crack branching and crack deflection. Furthermore, electrochemical and in-vitro immersion studies demonstrated that the corrosion behavior of Mg-3Zn composite under high concertation encapsulation was slightly reversed by fCNTs. Furthermore, cell culture investigations revealed that MG-63 cells present high level of cell viability and proliferate, implying that Mg-3Zn/0.4fCNTs composites are cytocompatible. All the findings suggest that the Mg-3Zn/0.4fCNTs composite with outstanding mechanical properties and appropriate

* Corresponding authors.
*E-mail addresses:* rezabakhsheshi@pmt.iaun.ac.ir (H.R. Bakhsheshi-Rad), filippo.berto@ntnu.no (F. Berto).

https://doi.org/10.1016/j.matdes.2021.110354

corrosion resistance and biocompatibility may be a potential candidate for biodegradable implant application.


## 1. Introduction

Magnesium (Mg), the lightest structural metal, has attracted the attention of researchers due to its excellent machinability, recyclability, electromagnetic shielding, damping response, specific mechanical characteristics and nutritional properties [1,2]. Mg has a lot of promising applications in automobiles, electronics, sports, aerospace and biomedicine components [3–5]. Mg has fundamental characteristics that are similar to those of human bone, such as density and elastic modulus. Moreover, corrosion products of Mg are not toxic to human physiology and they may even facilitate the growth and healing of human tissues [6]. However, compared to other light metals such as Al and Ti, Mg and its alloys have limited ambient temperature strength and ductility, which prevents widespread application in these fields [5]. Mg alloys have a great degradation rate and $H_2$ evolution in simulated body fluid (SBF), resulting in implant failure before the whole healing process [6]. Monolithic Mg is not employed directly in service settings because of these limitations, and alloying elements/secondary reinforcements are required to overcome these shortcomings and improve the properties of Mg [5,7,8]. The most popular procedure to improve mechanical and corrosion characteristics in Mg is alloying and composite preparation [5]. Because of their high specific strength and stiffness, magnesium-based composites reinforced with hard second phases have recently shown considerable promise for use in medical applications. Carbon nanotubes (CNTs) have received a lot of interest in various fields and they are particularly considered to be a good choice for multifunctional composites and engineering fields because of their attractive characteristics [2,3,9,10]. It has outstanding strength (30 GPa) and stiffness (1 TPa) in tension [11,12], great load transfer efficiency, chemical inertness, and high thermal conductivity (3000 W/m.K) [13], enabling it one of the best reinforcement materials for the fabrication of nanocomposites [13,14]. Furthermore, the CNT also has a high aspect ratio, which means it has a large surface area to volume ratio [14]. Because of its unique characteristics and the high surface area to volume (SA/V) ratio of CNT, it has been used with other materials to develop desirable composite materials [12]. Over the last 5 years, CNTs have received increased attention as super reinforcements for Mg alloys, with studies primarily focusing on their contribution to improving the mechanical properties and corrosion performance of microstructural components [14,15]. Despite numerous interesting studies on CNT-reinforced composites, Mg matrix composites containing CNT, particularly at high CNT concentrations, have not seen widespread application due to three critical challenges: (i) acquire CNT without defect in the consolidation process, (ii) distribution and dispersion of CNT in the matrix, and (iii) appropriate bonding at the matrix/CNT interface to achieve good load transfer between phases in the composite [14–16]. Nevertheless, due to the damage or uneven dispersion of carbon nanomaterials in the matrix, the improvement in strengthening efficiency is still undesirable. Acid-treated CNTs typically have a lot of oxygen-containing functional groups like hydroxyl and carboxyl [4]. These functional groups on carbon nanomaterials have been shown to improve interfacial strength between nanofillers and the matrix. Semi-powder metallurgy technique has been highly useful and investigated in order to increase the distribution of CNTs, provide homogenous properties, and enable the efficient utilization of the characteristics [4,9,16]. Subsequently, cold pressing and hot extrusion were used to consolidate the composite mixture. It is interesting that the extrusion process is an excellent technique to achieve greater material performance and promote the alignment of CNTs in the extrusion direction [17]. Hou et al. [18] showed that a considerable improvement in mechanical properties and thermal conductivity of Mg-based matrix was obtained by the uniform distribution of MWCNTs within the matrix of the composite. Zeng et al. [19] investigated the effects of CNTs on the microstructure and mechanical properties of Mg-2.0Zn alloy and their results showed that CNTs could refine the grain size of both as-cast alloy and as-extruded alloy. Huang et al. [20] fabricated Mg-6Zn/CNTs composites by stirring casting integrated with friction stir processing (FSP) and their results exhibited that the strength and elongation of the composite increased due to the grain refinement, Orowan looping and load transfer mechanisms. Mg-Zn/CNT composites was also prepared using powder metallurgy with different content of Zn element and CNTs reinforcement by Darsono et al. [21]. Their results showed that the fabricated samples exhibited a low corrosion rate, while the addition of more than 3 wt% CNTs has a reversed effect due to the lack of dispersion and segregation of CNTs in the grain boundaries resulting in an increase in the corrosion rate of the composite. So far, there are a few comprehensive reports on the incorporation CNTs on the biological and mechanical properties of extruded magnesium-based composites. The aim of this research was to develop Mg-3Zn/CNT composites with different CNTs concentrations using a combination of semi-powder metallurgy, sintering and extrusion processes. In the first part, the effect of CNTs and their contents on the microstructure and mechanical properties of the extruded Mg-3Zn/xfCNTs composites are studied. The corresponding strengthening mechanisms were discussed in detail. In addition, degradation properties were investigated by immersion tests and electrochemical measurements. Subsequently, the biological properties of the composites were evaluated using cell morphology, MTT assay and ALP activity.

## 2. Experimental procedure

### 2.1. Materials and composite fabrication process

Mg powder (99.8% purity, 50 μm mean particle size) and Zn powder (98.8% purity, 7.5 μm mean particle size) were bought from Sigma-Aldrich, USA. Multi-walled carbon nanotubes (MWCNTs) (8 nm in diameter, 5–10 μm in length, and 95% purity) as the starting reinforcement materials were supplied by Platonic Nanotech Pvt. Ltd. First Mg and Zn powders ball milled for 25 h in the planetary ball mill in argon atmosphere (< 3 ppm oxygen) with a 20:1 ball to powder ratio and a rotation speed of 300 rpm for fabrication of the Mg-3Zn alloy. To overcome the Van der Waals force between CNTs, functional groups such as carboxyl (–COOH) and hydroxyl (–OH) were introduced at the CNTs surface by immersing CNTs to a mixture of $H_2SO_4$ and $HNO_3$ (1:3 by volume) at 40 °C for 4 h. The slurry was filtered and washed with distilled water and ethanol. The Mg-3Zn/xfCNTs (x = 0, 0.2, 0.4 and 0.8 wt %) composites were synthesized using semi powder metallurgy technique (as shown in Fig. 1). The ball-milled magnesium alloy was mixed in ethanol for 1 h by means of magnetic stirring at 600 rpm for 1 h. At the same time, the MWCNTs with functional groups (fCNTs) were ultrasonicated separately in ethanol for 1 h.


**Fig. 1.** Schematic view of the preparation process of Mg-3Zn/fCNTs nanocomposites.

A drop of a specific solution of fCNTs was applied to the above powder slurry in ethanol at a speed of 600 rpm for 3 h. To acquire the composite powder, the mechanically agitated mixture was filtered and vacuum dried in a vacuum oven at 343 k for 24 h. The annealed mixture was compacted in a steel mold 10 mm in diameter under a pressure of 650 MPa to obtain the green compacts. Next, the green compacts were sintered for 2 h in a tube furnace at 873 K in an argon atmosphere. Then the sintered compacts were hot extruded at a speed of 2 mm/s with an extrusion ratio of 16:1 via a 100 ton hydraulic press [5].

### 2.2. Microtructural characterization

A field emission scanning electron microscope (FESEM, Tescan, Mira 3 Czech Republic) was used to perform microstructural and fractographical characterizations. The instrument was equipped with an energy-dispersive X-ray spectroscopy detector (EDS, DXPeX10 P Digital X-Ray Processor). The X-ray diffraction (Siemens D5000) with Cu-Kα radiation (45 kV, 40 mA) was applied to reveal the phase components. Transmission electron microscopy (TEM; Phillips 208 m) was used to investigate the morphology of CNTs, milled matrix powder and composite powders. A Raman spectrometer (Takram P50C0R10 with a laser wavelength of 532 nm) was employed to determine the structural changes of CNTs in the nanocomposites.

### 2.3. Mechanical properties

The compression behavior of sintered samples with a diameter of 6 mm and a height of 9 mm was measured on cylindrical sintered nanocomposites at room temperature in conjunction with ASTM-E9-09 using the SANTAM (STM-50) universal testing machine at a constant crosshead speed of 0.5 mm/min. For the determination of compressive strengths, the stress-strain curves were reported and used. Indentation tests were conducted using a Vickers hardness tester (LECO M-400) on the sintered samples at a peak load of 300 gf and a duration of 15 s. For the average value, each specimen was analyzed in five various locations.

### 2.4. Corrosion behavior

The immersion and electrochemical methods were employed to measure the corrosion properties of nanocomposites. The corrosion tests were performed in the simulated body fluid (SBF). Kokubo's solution [22] was used as the SBF solution with chemical composition as listed in Table S1 (presented in the supporting information). Before the corrosion measurement started, the surface of prepared specimens was ground with 600–2000 grade SiC abrasive paper and then sonicated in an acetone bath for 3 min. Finally, it was dried in a stream of hot air. A potentiometric polarization test with an EC-Lab machine at a voltage range of −250 to +250 $mV_{SCE}$ and an open circuit potential at a rate of 0.5 mV/s in the SBF was performed to evaluate the corrosion rate. A saturated calomel electrode (SCE) was used as the reference electrode, and a graphite electrode was used as the counter electrode. The samples were examined with a certain surface of 0.785 $cm^2$ exposed to an electrolyte as the working electrode. Electrochemical impedance spectrometry (EIS) was employed after 30 min immersion of the composites in SBF to obtain stability in the potential. This test was performed at an open circuit potential in the range of $10^5$ to $10^{-2}$ Hz, in accordance with the ASTM G106 standard, using a sinusoidal signal with a potential amplitude of 10 mV. In order to study the bioactivity behavior, each of the Mg-3Zn/xfCNTs nanocomposites was immersed in 100 mL SBF at 37 °C for 7 days. They were removed from the SBF cups after the period, rinsed with distilled water and dried in the open air.

### 2.5. In-vitro bioactivity and cell culture tests

A direct cell adhesive assay was carried out for samples. Initially, in a Dulbecco's modified Eagle medium (DMEM) containing 10% Fetal Bovine Serum (FBS), 1% penicillin/ streptomycin and 1.5% Geneticin human osteogenic sarcoma MG-63 line cells were cultivated under the standard cell-culture conditions. In 12-well plates, 1 mL MG-63 cells with a density of $3 \times 10^4$ cells/mL were distributed to the composites and cultured for 24 h. The composites were then taken out from the plate upon immersion and washed two times with PBS. The cells attached to the composite surface were fixed with 2.5% glutaraldehyde and dehydrated in 70% etha-

nol for 2 h and subsequently, the cell morphology was evaluated according to the Ref [23]. An indirect 3-(4,5-dimethylthiazol −2-yl)-2,5-diphenyltetra-zolium-bromide (MTT, Sigma, Saint Louis, USA) assay based on the extraction technique was used to evaluate the in vitro nanocomposite cytotoxicity comprising fCNTs. The nanocomposites were applied to the culture medium and immersed at 37 °C for 24 and 48 h. The MG-63 cells were seeded in 96 well culture plates with $10^4$ cells/mL of medium in each well and the plates were incubated with 5 % $CO_2$ inside the incubator for 24 h and 48 h at 37 °C in the humidified atmosphere, following the Ref [24]. Nuclear staining with DAPI (4′, 6-diamidino-2-phenylindole, blue fluorescence in live cells) was performed to study the MG-63 cell line proliferation nanocomposites containing fCNTs under fluorescence microscopy. The cell viabilities were determined by:

$$\text{Cell Viability}\,(\%) = \left(\text{OD}_{\text{sample}}/\text{OD}_{\text{negative control}}\right) \times 100$$

Where OD as measured with a fluorescence microscope, is optical density. The optical density of the sample and the negative control are denoted by $\text{OD}_{\text{sample}}$ and $\text{OD}_{\text{negative control}}$, respectively. Besides, an alkaline phosphatase (ALP) staining process was conducted to assess the differentiation capability of MG-63 cells in 24 h and 48 h post-culture extracts. The cultured cells were washed with PBS 3 times and then fixed with 4% paraformaldehyde for 30 min. After washing 3 times with PBS, they were stained with ALP staining reagents. The stained cells were washed by PBS three times after holding the cells overnight at 4 °C, and then detected by an optical microscope.

### 2.6. Statistical data analysis

All data obtained are expressed as mean value ± standard deviation (SD) (for n = 3). T-tests were performed between various groups to assess the p values that were considered to be significant when $^{*}p < 0.05$ and $^{**}p < 0.01$ were used.

## 3. Results and discussion

### 3.1. Microstructural characteristics

The morphologies of pure Mg, pure Zn, fCNTs, Mg-3Zn alloy and Mg-3Zn/fCNTs mixed powders were observed using FE-SEM as presented in Fig. 2. The FE-SEM images revealed that all Mg powders have irregular shapes and Zn powders possess spherical shapes (Fig. 1a,b), while the latter exhibited much finer particles. The particles size distribution was quantified. In SEM (Fig. 2d,e) and TEM (Fig. 2f) micrographs, a variation in powder size was found for ball-milled alloy powder with an average value in the range of 40 to 200 nm, whereas particle sizes for Mg and Zn powders were around 50 ± 5 μm and 7.5 ± 0.5 μm, respectively (Fig. 2a, b). In the as-received condition, the clustered morphology of fCNTs is substantially tangled together, as shown in Fig. 2c. The TEM image confirmed that fCNTs have a mean diameter of 8 nm and a length of 5–10 μm in this regard (Fig. 2g). Fig. 2h,i shows the FE-SEM image of the Mg-3Zn/0.4fCNTs nanocomposite powders. The fCNTs are adequately inserted and strongly held to the Mg-3Zn ball-milled alloy matrix, as can be shown, implying that the fCNTs and the Mg-3Zn matrix have strong interfacial bonding. In addition, it shows the presence of fCNTs in the matrix, which are uniformly distributed in the matrix with a different structure [25].

Fig. 3a,b shows the TEM images of the mixed Mg-3Zn/0.4fCNTs powders. The fCNTs were individually adhered to the surfaces of Mg-based powders, as seen in the enlarged image of the square region in Fig. 3a,b. As shown in Fig. 3a,b implies that unbound fCNTs were completely wrapped around the ball-milled Mg-based powders. The EDS analysis of the Mg-3Zn/0.4fCNTs nanocomposite exhibits that the elements of C, Mg, Zn and O are included (Fig. 3c), which is compatible with the construction of Mg-3Zn/fCNTs. Furthermore, no dispersion molecule elements like sulfur were found, indicating that the dispersant was totally eliminated during the annealing process. This suggests that the established approach for synthesizing mixed Mg-3Zn/fCNTs powders with uniformly distributed fCNTs is effective [5]. When the surface of Mg comes into contact with a relative oxygen-rich environment of CNT, the relatively low oxygen concentration supplied by functional groups on fCNTs is responsible for the formation of MgO. Based on an atomic view, Fig. 3d depicts the production process of MgO nanoparticles at the Mg-fCNT interface. The nucleation of oxide islands on the Mg particles surface will continue until the island saturation density is attained. Following the coalescence of the islands, oxide development occurs by interfacial oxygen diffusion, resulting in interfacial MgO with a cubic structure. The in-situ produced MgO nanoparticle not only provides strong interfacial interaction between the Mg matrix and the reinforcement, but it can also inhibit dislocation motion by the generation of dislocation loop. As a result, the interaction between MgO and dislocations contributed to the enhanced strength of the current composites via the Orowan mechanism. Furthermore, the presence of oxygen-containing functional groups at the contact could increase the development of Mg oxide at the interface, hence improving load transfer efficiency by change the mechanical bonding into chemical bonding at the interface [26,27]

The elemental mappings of the Mg-3Zn/0.4fCNTs composite are shown in Fig. 4. It implies that the C element was distributed homogeneously, implying that the fCNTs were distributed uniformly in the Mg-3Zn/0.4fCNTs composite. The XRD patterns of Mg-3Zn alloy and the composite comprising CNTs are shown in Fig. 5a. This graphic clearly shows α-Mg, $Mg_7Zn_3$ and fCNTs diffraction peaks of the composite sample. Scanning electron microscopic analysis in Fig. 4e revealed that $Mg_7Zn_3$ phases precipitate in grains were detected in Mg-3Zn/0.4fCNTs nanocomposite. Also, the X-ray diffraction patterns of Mg-based matrix alloy and Mg-3Zn/0.4fCNTs nanocomposites showed the presence of peak related to the $Mg_7Zn_3$ intermetallic phase as presented in Fig. 5a. Also the existence of α-Mg and $Mg_7Zn_3$ peaks indicates that eutectic transformations occurred during the milling and sintering processes. The corrosion resistance and mechanical strength of Mg-based alloys could be improved by these intermetallic phases [28].

The variation of basal texture due to the addition of reinforcement in extruded Mg-based materials can also affect strengthening [29]. According to XRD patterns of Mg-Zn alloy and developed composites in Fig. 5a, the presence of fCNTs leads to a reduction of basal texture. Zhang et al. [30] fabricated the Mg-Zn alloy in the variation of Zn contents by casting method, and MgZn phase patterns were identified for alloys with Zn mass fractions greater than 5%. Also, the XRD patterns of samples clearly displayed MgO peaks, indicating that the bare alloy and nanocomposites were partially oxidized, as shown in Fig. 5a. Furthermore, the literature suggests that Mg is highly prone to oxidation in an oxygen-rich environment. As a result, if there is enough oxygen ($O_2$) in the composite, a thin MgO layer will eventually form on the Mg particles [7,17,18]. The presence of oxygen atoms in the internal grain boundaries of the composites reacted with Mg matrices at about 410 °C and MgO was produced [31]. Mechanical characteristics can be related to the activity of basal slip and twinning influenced by the texture. Magnesium materials usually have a strong basal texture, which limits material deformability. The presence of the second phase in the Mg alloy can affect the variations in the intensity of the basal, prismatic, and pyramidal planes, and randomization of basal texture was shown to improve the ductility of magnesium materials [32–34]. As a result, XRD patterns of the

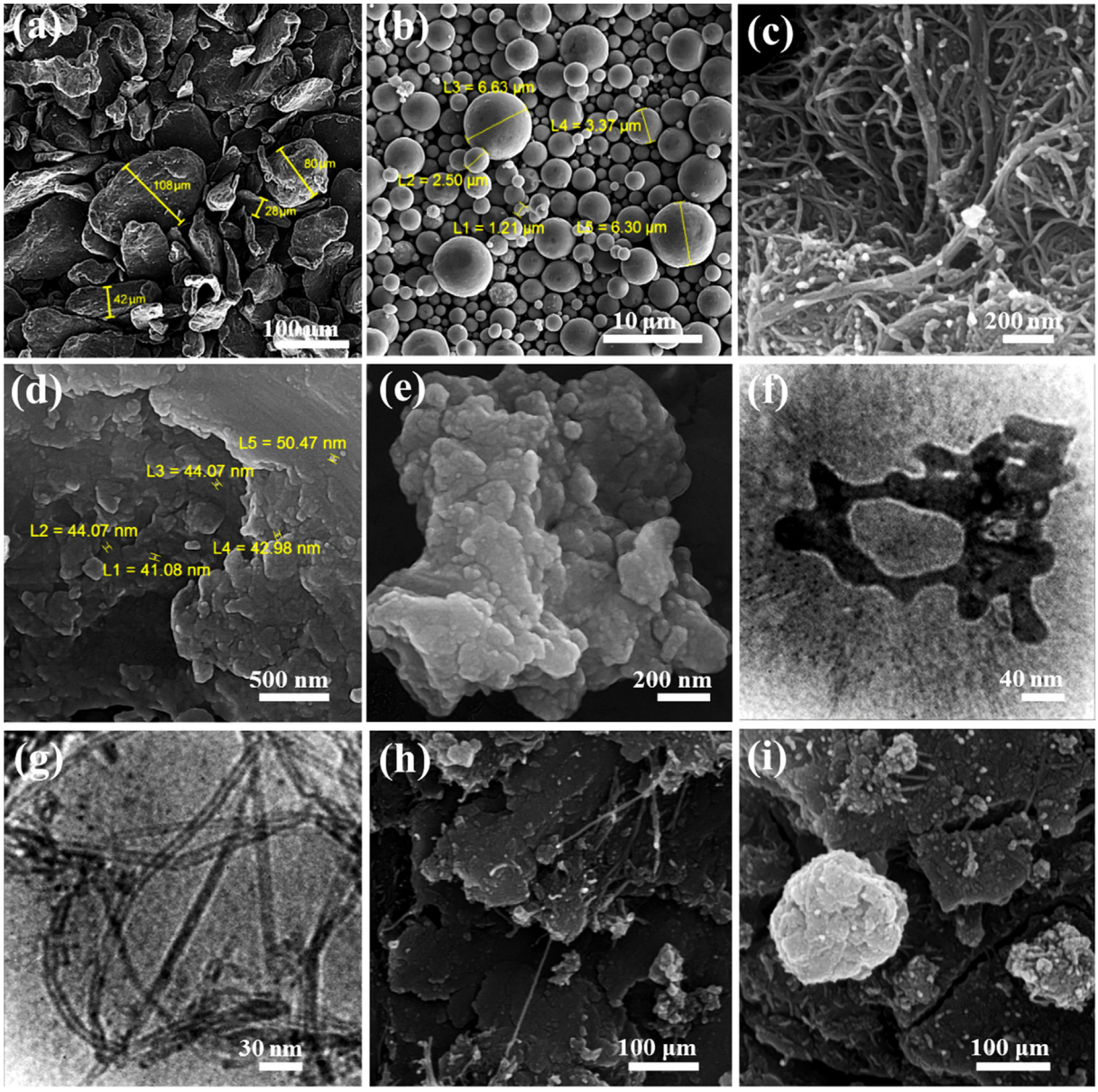


**Fig. 2.** FE-SEM micrographs of (a) pure Mg, (b) pure Zn, (c) fCNTs, (d,e) Mg-3Zn ball-milled alloy in different magnifications, TEM micrographs of (f) Mg-3Zn ball-milled alloy and (g) fCNTs and (h,i) FE-SEM micrographs of Mg-3Zn/0.4fCNTs composite powder.

Mg-3Zn alloy and the developed Mg-3Zn/0.4fCNTs composite show obviously decreasing the intensity of basal planes multiples of random distribution, as shown in Table 1. The presence of fCNTs reduces basal texture, according to XRD patterns. The randomization of basal texture could be caused by the encounter of Mg-3Zn alloy deformed through uniform dispersion of CNT, which causes grain rotation and reduces texture intensity. Raman spectrum investigation revealed the presence of fCNTs in the Mg-3Zn/0.4fCNTs composite (Fig. 5b). The peak at 1351.13 $cm^{-1}$ (D-band) matched carbon atom vibration at disordered graphite in-plane termination. The $sp^2$ bonded carbon atom vibration in the 2D hexagonal lattice was responsible for the peak at 1590.63 $cm^{-1}$ (G-band) [35]. The spectra of Mg-3Zn/0.4fCNTs composites showed the aforementioned peaks, showing that fCNTs survived the sintering and subsequent extrusion processing. The integrated intensity of the D and G bands ($I_D/I_G$) measures the degree of defect in fCNTs; the higher the ratio, the more defects are present [5]. As demonstrated in Fig. 5b, the intensity ratio of $I_D/I_G$ for Mg-Zn/0.4fCNTs composites was 1.22, which was close to that of the fCNTs powder. According to the findings, the SPM method did not induce significant defects in the structure of fCNTs [35].

To further verify whether CNT plays a role in the grain refinement of Mg-3Zn alloy, we studied the optical images of the composites, as shown in Fig. 5c. As is obvious from this figure, with the increasing amount of the fCNTs content from 0 to 0.8 wt%, the mean grain size of the composites has diminished slightly. It was reported [29] that using extrusion as a secondary process reduces defects and grain size and results in a more homogeneous reinforcement distribution. Extrusion is a widely accepted post-forming process used on Mg alloys at high temperatures to improve their properties. Dynamic recrystallization (DRX) operation develops fine grain microstructure during the forming process. The microstructures of the extruded alloy sample compared to the un-extruded matrix are shown in Fig. 5c shows a significant reduction of grain size from 76 to 13.4 µm.

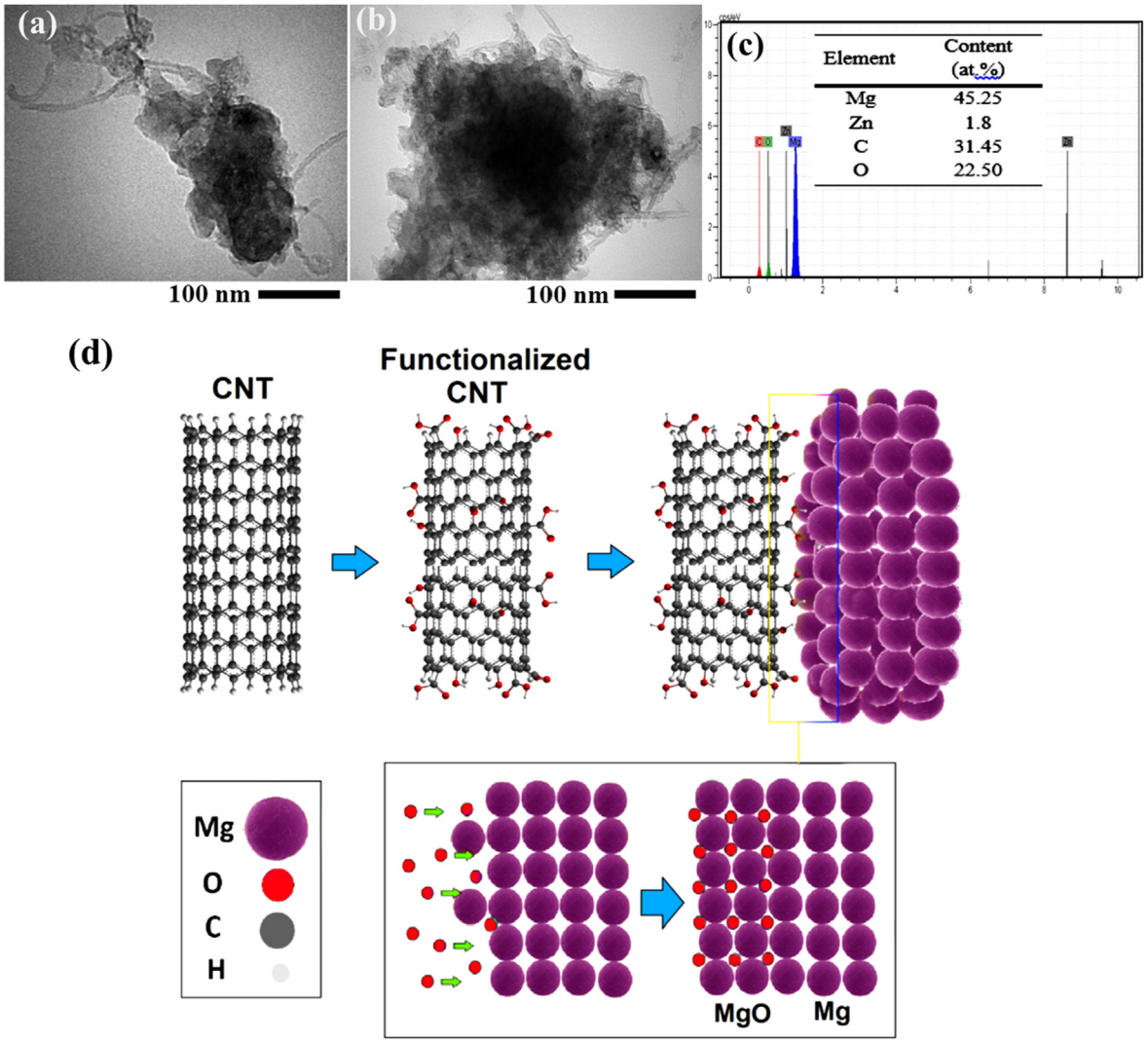


**Fig. 3.** (a,b) TEM images of Mg-3Zn/0.4fCNTs composite, (c) EDS results of Mg-3Zn/0.4fCNTs nanocomposite powder, (d) Schematic illustrations the oxygen-mediated bonding between Mg and fCNTs.

### 3.2. Mechanical properties

Fig. 6a shows the microhardness of Mg-3Zn/fCNTs composites. As demonstrated, the microhardness gradually escalated as the amount of fCNTs in the sample increased from 0 to 0.8 wt%. Another criterion for bone implants was compression strength [1]. Fig. 6b illustrates the compression strength of Mg-3Zn/fCNTs composites. Mg-3Zn/0.2fCNTs, Mg-3Zn/0.4fCNTs and Mg-3Zn/0.8fCNTs composites showed high compression strength of 368.2, 390 and 320.2 MPa and hardness of 70, 74 and 76 HV, respectively, in comparison with Mg-3Zn (289.6 MPa and 66 HV). It could be found that fCNTs (0.2–0.8 wt%) increased the compression strength of Mg-based alloy, providing adequate mechanical support for the human compact bone to withstand flexural pressure after implantation [36]. Ultimate compressive strength (UCS) and strain to failure demonstrate that Mg-3Zn reinforced with fCNTs is stiffer than Mg-3Zn composites (Fig. 6b and Table 2). The following factors may contribute to the increase in microhardness, UCS, yield strength (YS), and strain to failure of Mg-3Zn/fCNTs composites: (i) dislocation reproduction caused by mismatch in the coefficient of thermal expansions (CTE) between reinforcement (CNTs) and the matrix, (ii) grain refinement, (iii) Orowan mechanism, and (iv) efficient load transfer from the matrix to the second phase [25,37]. In the case of Mg-3Zn/0.8fCNTs, agglomeration of fCNTs, as well as pores in the composite, might operate as a source of stress concentration points and cracks that spread quickly, leading the composite failure [6,20]. As a result, the mechanical characteristics of the composite containing a high amount of CNT were reduced. The strengthening mechanism is indicated through a schematic diagram shown in Fig. 6c. Uniform distribution of CNTs within Mg-3Zn alloy and subsequently producing a large interconnected network of nano-fillers in the matrix, thus leading to further grain refinement and enhancement of mechanical properties. However, agglomeration of CNTs with a large aspect ratio in Mg-3Zn alloy would cause accumulation of dislocation, which leads to crack formation and reduced compressive failure strain. In fact, uniform dispersion of the nanoscale CNTs in the Mg-3Zn matrix carbon nanotube could restrict the dislocation motion during mechanical testing, as shown in Fig. 6c, resulting in increased strength. When the shear stress on the dislocation increases, it can migrate across the second phase particle by cutting or bypassing the local stress concentration, resulting in higher plastic deformation and improved ductility behavior. Furthermore, the dispersion of nanoscale second phase in Mg alloys could result in a decreased basal texture, improving the ductility of Mg-3Zn/CNT composites [5,38]. In this respect, according to [12] that load

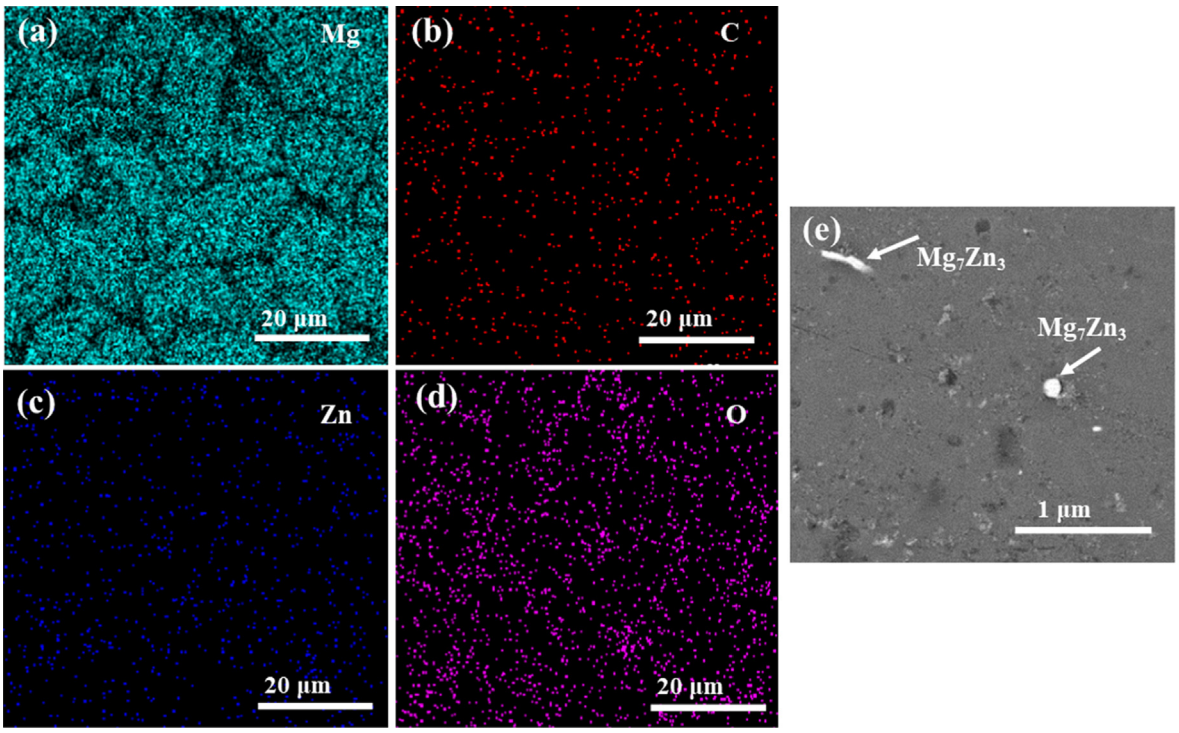


**Fig. 4.** EDS of Mg-3Zn/0.4fCNTs composite showing elemental mapping: (a) - Mg element, (b) C element, (c) Zn element, (d) O element, and (e) SEM images of Mg-3Zn/0.4fCNTs composite showing intermetallic phase of $Mg_7Zn_3$ embedded in composite matrix.

transfer strengthening is the most dominant strengthening mechanism of CNTs in the Mg-based matrix since CNTs have the unique capacity to support high loads during composite failure tests, resulting in superior mechanical properties. The most important factor for good load transfer from the soft matrix to the hard second phase is strong interfacial bonding between CNTs and matrix [5,39]. Furthermore, the addition of CNTs improves the ductility of Mg-based composites by boosting basal slip, as CNTs can enhance twin formation and weaken the predominant basal texture in Mg matrix composites. Besides, the relatively uniform dispersion of CNTs and local stresses formed by the reinforcement addition boost non-basal slip, resulting in an increase in failure strain [5,38].

FE-SEM was used to characterize the cracks in order to determine the mechanism responsible for the improved mechanical characteristics (Fig. 6d-g). Fig. 6d showed the presence of fCNTs crack bridging on the cracks (labeled by yellow arrows). Individual CNTs bridged the gap between the crack surfaces, preventing the Mg matrix from rupturing. Characteristic crack branching and crack deflections could be seen in Fig. 6e and g, respectively. The crack first propagated in its own plane, then along the fCNT–Mg interface when it came into contact with fCNT, followed by a deflection to the Mg matrix. These mechanisms occurred several times in the propagating path and would create a complex pathway to release stress, which could reinforce the Mg matrix.

The FE-SEM image reveals considerable fCNT pull out on the fracture surface (Fig. 6g). This implies that the influence of fCNTs on dislocation obstructions and bridging is favorable to load transfer and increases the bearing capacity of the matrix, which played a vital role in strengthening and improving malleability to certain extent [13]. The addition of fCNTs into the matrix of Mg alloy has been demonstrated to affect the ductility of Mg-based composites by boosting the slip systems activated by fCNTs [25,38]. Furthermore, some ruptured fCNTs were detected individually exposed outside the fractured surface in Fig. 6g (yellow arrows), revealing that load transfer was effective [25].

Table 2 summarizes the results of mechanical characteristics tests, including UCS, failure strain, and hardness. Table 2 summarizes the results of mechanical characteristics tests, including UCS, failure strain, and hardness. In order to make a comparison, the results are compared to the Mg-based composites containing fCNTs and their derivatives for a better understanding of the mechanical properties of the fabricated composite. As reported in the recent studies, small incorporation of fCNTs can lead to notable improvement in mechanical characteristics due to their high surface area; the small concentrations of 0.2–0.8 wt% were chosen as reinforcement in this investigation. Also, lower amounts of CNT loading can limit the probability of reinforcement agglomeration and prohibit chemical or physical interference during the development of Mg-based composite [5]. The content of CNTs in the Mg-based microstructure was related to the dispersion and loading of functional groups on CNTs [40]. Besides, Zanello et al. [41] demonstrated that implantation of CNTs in the bone could improve the mechanical properties of damaged bone tissue. According to this perspective, the homogeneous distribution of fCNTs into the matrix reduced the propagation of cracks in Mg-based composites under static and dynamic loadings. The results demonstrated that introducing CNT to the Mg-based composite might improve both the bending and tensile strengths of the final nanocomposite [12,40]. Based on the findings, it is possible to conclude that the improvement in mechanical properties is due to CNTs arresting and delaying crack propagation in the Mg-based composite via a bridging effect and that obstructing crack propagation resulted in a properly homogeneous distribution of CNT in the Mg-based composite, which can attract and delay crack propagation in the composite. In degradable orthopedic implants, a desirable biodegradable material must have a strength of more than 200 MPa and an elongation larger than 10% to attain an efficient service life of 90–180 days [42]. In overall, the results show that the compressive strength of Mg-3Zn/0.4fCNTs (390 ± 15 MPa) is higher compared to Mg-3Zn/15HA (257.3 ± 5.4 MPa) [43], Mg-3Zn-5HA (134 ± 3 MPa) [44], Mg-3Zn-0.5Ag (190.9 MPa) [45],

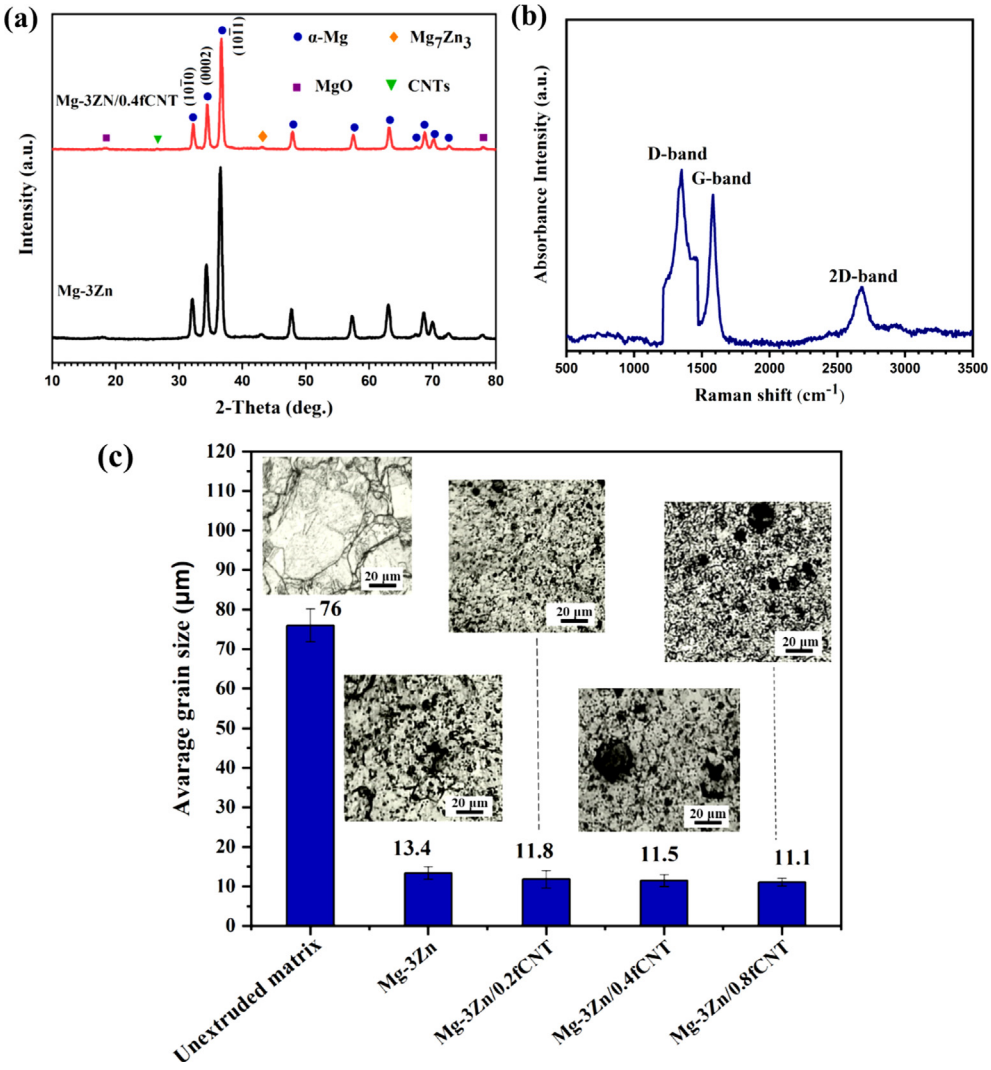


**Fig. 5.** (a) XRD pattern of Mg-3Zn alloy and Mg-3Zn/0.4fCNTs composite, (b) Raman spectra of the fCNTs reinforced Mg nanocomposite, (c) OM image and grain size calculations of unextruded Mg-3Zn alloy matrix and extruded Mg-3Zn/xfCNTs (x = 0, 0.2, 0.4 and 0.8 wt% fCNTs) composites.

**Table 1**
Variations of the intensity ratio of basal planes multiples of random distribution.

| Materials | I (0002) / I (1011) |
|---|---|
| Mg-3Zn | 0.43 |
| Mg-3Zn/0.4fCNTs | 0.40 |

Mg-2.5$TiO_2$ (305.5 ± 11 MPa) [46] and cortical bone (164–240 MPa) [47], which meet the requirement for biomedical applications.

Fig. 7 shows SEM images of the fracture surface of the matrix and nanocomposites. The obtained results in the fracture surface demonstrate in Fig. 7a that there is a combination of cleavage platform and dimples. The dimples shown in Fig. 7b,c reveal that the fractures in the nanocomposite containing 0.2 and 0.4 wt% of fCNTs are ductile, while in the nanocomposite containing higher wt.% of fCNTs (0.8 wt%) reveals a typical crack detected from the fracture surface. It can be seen that the crack goes principally along the grain boundary, implying that the fracture was started by microcracks that developed along the grain boundary. This relatively more ductile compressive fracture behavior of nanocomposite containing moderate content of fCNTs can be attributed to increase in shear band spacing [12].

### 3.3. Corrosion behavior

Fig. 8 presents the results of the Mg-3Zn/xfCNTs (x = 0, 0.2, 0.4 and 0.8 wt%) composites after their immersion tests. According to the immersion test results, the fCNTs addition has a slight effect on the corrosion resistance of the composites up to 0.4 wt%, beyond which the corrosion considerably increased. Compared with Mg-3Zn, the corrosion of Mg-3Zn/0.2fCNTs and Mg-3Zn/0.4fCNTs nanocomposites in SBF were intensified and a great many cauliflower-like corrosion compounds precipitated on the surface, particularly Mg-3Zn/0.4fCNTs composite. As illustrated in Fig. 8c, after 7 days of immersion, the Mg composite containing 0.8 wt% fCNTs corroded severely, causing the composite to partially collapse. The cauliflower type structure is also produced in Mg-3Zn/0.8fCNT by increasing the amount of fCNTs. As a result, increasing the amount of fCNTs to 0.4 wt% causes the cauliflower type structure to grow and become preferentially oriented in the Mg-3Zn/fCNTs composite. Also, the EDS analysis on points A to C indicates an escalation in the atomic percentage of phosphorus, suggesting the positive growth of the apatite film on the composites with the increasing fCNTs content.

The morphology of all Mg-3Zn/fCNTs demonstrates that some hydroxyapatite regions reshaped from aggregation to plate shape,

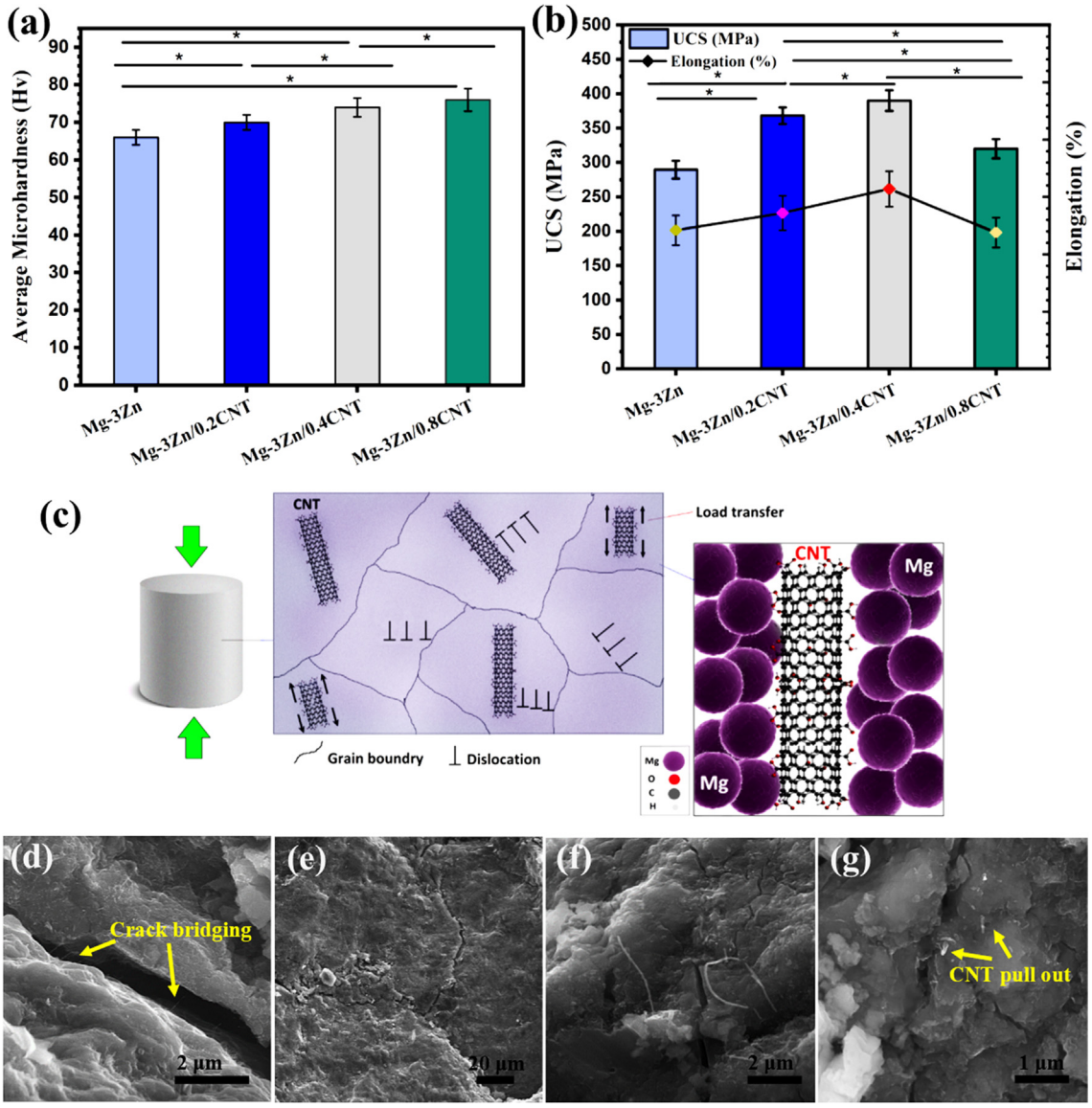


**Fig. 6.** (a) Microhardness values of composites, (b) Values of ultimate compressive strength (UCS) and failure strain of Mg-3Zn/xfCNTs (x = 0, 0.2, 0.4 and 0.8 wt.% fCNTs) composites, (c) Schematic diagram showing the dislocations pinned by CNTs, FE-SEM images of (d) crack bridging, (e) crack branching, (f) crack deflection and (g) fCNTs pull out.

resulting in structure homogeneity. It is possible that the fCNTs will agglomerate in some regions, resulting in more nucleation sites. Besides that, fCNTs may regulate the growth direction of HA crystals, causing a cauliflower-like structure with a particular direction to develop. In contrast, the hydroxyapatite morphology remains in aggregation and cauliflower type structure in regions with a lower content of fCNTs. As mentioned earlier, the addition of fCNTs had an effect on HA morphology because fCNTs particles can control both nucleation and crystal growth of HA crystals. In more detail, the negatively charged carboxyl groups of fCNTs can operate as a nucleation site, attracting $Ca^{2+}$ ions, which causes the adsorption of $PO_4^{3-}$ or $HPO_4^{2-}$, eventually leading to the formation of HA. Based on equations of (1) to (4), the degradation rate of Mg was also controlled by the volume of hydrogen gas evolution and the released $Mg^{2+}$ and $OH^-$ ions. As a result, $Mg(OH)_2$ is produced on the surface of Mg alloy:

Anodic reaction:

$$Mg_{(s)} \rightarrow Mg^{2+}{}_{(aq)} + 2e^- \quad (1)$$

Cathodic reaction:

$$2H_2O\ (l) + 2H^+{}_{(aq)} + 2OH^- \quad (2)$$

$$2H^+\ (aq) + 2e^- \rightarrow H_2\ (g) \quad (3)$$

Formation of corrosion products:

$$Mg^{2+}{}_{(aq)} + 2OH^-\ (aq) \rightarrow Mg(OH)_2\ (solid) \quad (4)$$

On the other side, the initially $OH^-$ generated by Mg degradation can directly react with the $HPO_4^{2-}$ in physiological solutions according to equation (5), resulting in the generation of $PO_4^{3-}$.

$$HPO_4{}^{2-}{}_{(aq)} + OH^-{}_{(aq)} \rightarrow PO_4{}^{3-}{}_{(aq)} + H_2O_{(l)} \quad (5)$$

Subsequently, the $PO_4^{3-}$ is reacted with the $Ca^{2+}$ in physiological fluid or $Mg^{2+}$ on the composite surface to deposit apatite or Mg–P compounds [50]. Other studies which use different techniques to make hydroxyapatite-fCNTs composites have expressed similar observations [6,51]. Besides, it is observed that fCNTs bridge

**Table 2**
Comparison of mechanical properties of Mg-3Zn/fCNTs composites with previous studies.

| Sample | Fabrication Method | E (GPa) | UCS (MPa) | Failure Strain (%) | Hardness (HV) | Ref. |
|---|---|---|---|---|---|---|
| Mg-3Zn | SPM followed by hot extrusion | 15.06 ± 2.5 | 289.6 ± 13 | 12.1 ± 1.3 | 66 ± 2 | This work |
| Mg-3Zn /0.2fCNTs | SPM followed by hot extrusion | 28.47 ± 1.3 | 368.2 ± 12 | 13.6 ± 1.5 | 70 ± 2 | This work |
| Mg-3Zn /0.4fCNTs | SPM followed by hot extrusion | 27.32 ± 2.3 | 390 ± 15 | 15.7 ± 1.5 | 74 ± 2.5 | This work |
| Mg-3Zn /0.8fCNTs | SPM followed by hot extrusion | 21.94 ± 1.4 | 320.2 ± 14 | 11.9 ± 1.3 | 76 ± 3 | This work |
| Mg-3Zn | SPS | _ | 217.2 ± 4.4 | 13.1 | ~75 | [43] |
| Mg-3Zn/5HA | SPS | _ | 230.1 ± 5.9 | 14.6 | ~86 | [43] |
| Mg-3Zn/10HA | SPS | _ | 242 ± 2.7 | 16.1 | ~97 | [43] |
| Mg-3Zn/15HA | SPS | _ | 257.3 ± 5.4 | 17.5 | ~105 | [43] |
| Mg-3Zn/20HA | SPS | _ | 207.2 ± 4.3 | 13.2 | ~77 | [43] |
| Mg-3Zn | SPM | _ | 130 ± 4 | 15 ± 1 | _ | [44] |
| Mg-3Zn-2HA | SPM | _ | 131 ± 6 | 14 ± 1 | _ | [44] |
| Mg-3Zn-5HA | SPM | _ | 134 ± 3 | 16 ± 1 | _ | [44] |
| Mg-3Zn-10HA | SPM | _ | 116 ± 5 | 17 ± 1 | _ | [44] |
| Mg-3Zn | PM | _ | 187.3 | 11.7 | ~60 | [45] |
| Mg-3Zn-0.5Ag | PM | _ | 190.9 | 11.9 | ~65 | [45] |
| Mg-3Zn-1Ag | PM | _ | 174.3 | 10.9 | ~73 | [45] |
| Mg-3Zn-2Ag | PM | _ | 166.7 | 9.9 | ~74 | [45] |
| Mg-3Zn-3Ag | PM | _ | 159.6 | 8.7 | ~77 | [45] |
| Mg | PM followed by hot extrusion | _ | 239 ± 15 | 19.8 ± 1.7 | 40 ± 2 | [48] |
| Mg/0.5Al-0.18CNT | PM followed by hot extrusion | _ | 357 ± 13 | 11.0 ± 1.3 | 50 ± 4 | [48] |
| Mg/1Al-0.18CNT | PM followed by hot extrusion | _ | 421 ± 15 | 12.5 ± 1.0 | 58 ± 3 | [48] |
| Mg/1.50Al-0.18CNT | PM followed by hot extrusion | _ | 421 ± 11 | 11.3 ± 1.7 | 60 ± 4 | [48] |
| AZ91-0.1 MWCNTs | Stir Casting | _ | 412 | 24.4 | _ | [39] |
| Mg–0HAp | Melting and extrusion | _ | 277.8 | _ | ~33 | [49] |
| Mg–15HAp | Melting and extrusion | _ | 298.2 | _ | ~68 | [49] |
| ZM61–0 HAp | Melting and extrusion | _ | 355.6 | _ | ~68 | [49] |
| ZM61–15 HAp | Melting and extrusion | _ | 388.3 | _ | ~95 | [49] |
| Mg | DMD followed by hot extrusion | _ | 332 ± 10 | 18 | 52 ± 1.5 | [46] |
| Mg-0.58$TiO_2$ | DMD followed by hot extrusion | _ | 285 ± 13 | 22.6 ± 1 | 58 ± 2 | [46] |
| Mg-0.97$TiO_2$ | DMD followed by hot extrusion | _ | 278.4 ± 8 | 22.5 ± 1.5 | 61 ± 2 | [46] |
| Mg-1.98$TiO_2$ | DMD followed by hot extrusion | _ | 297 ± 1 | 21.9 ± 1 | 64 ± 3 | [46] |
| Mg-2.5$TiO_2$ | DMD followed by hot extrusion | _ | 305.5 ± 11 | 22 ± 2 | 68 ± 1.5 | [46] |

SPM: Semi powder metallurgy, PM: Powder metallurgy, SPS: Spark plasma sintering, DMD: Disintegrated melt deposition, UCS: Ultimate compressive strength, E: Elastic modulus.

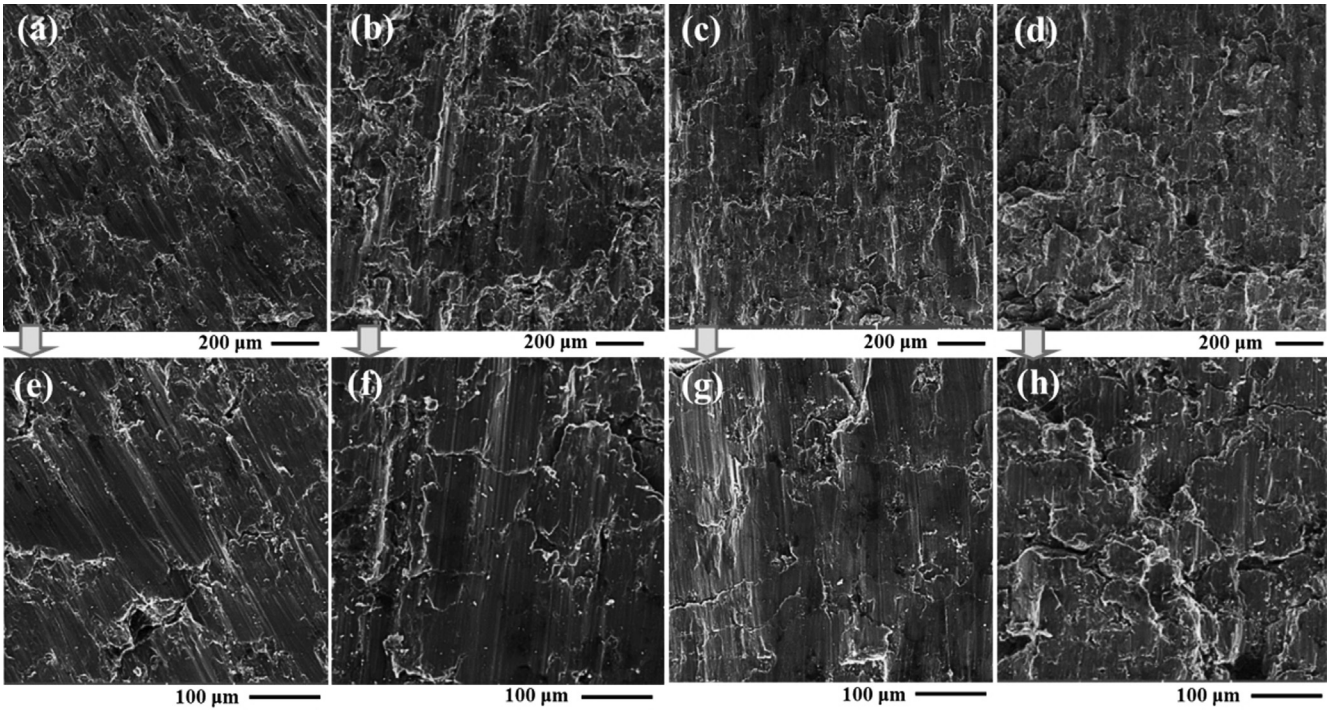


**Fig. 7.** SEM images of fracture surfaces of Mg matrix and composites after compression test: (a,e) Mg-3Zn alloy, (b,f) Mg-3Zn/0.2fCNTs, (c,g) Mg-3Zn/0.4fCNTs and (d,h) Mg-3Zn/0.8fCNTs nanocomposites.

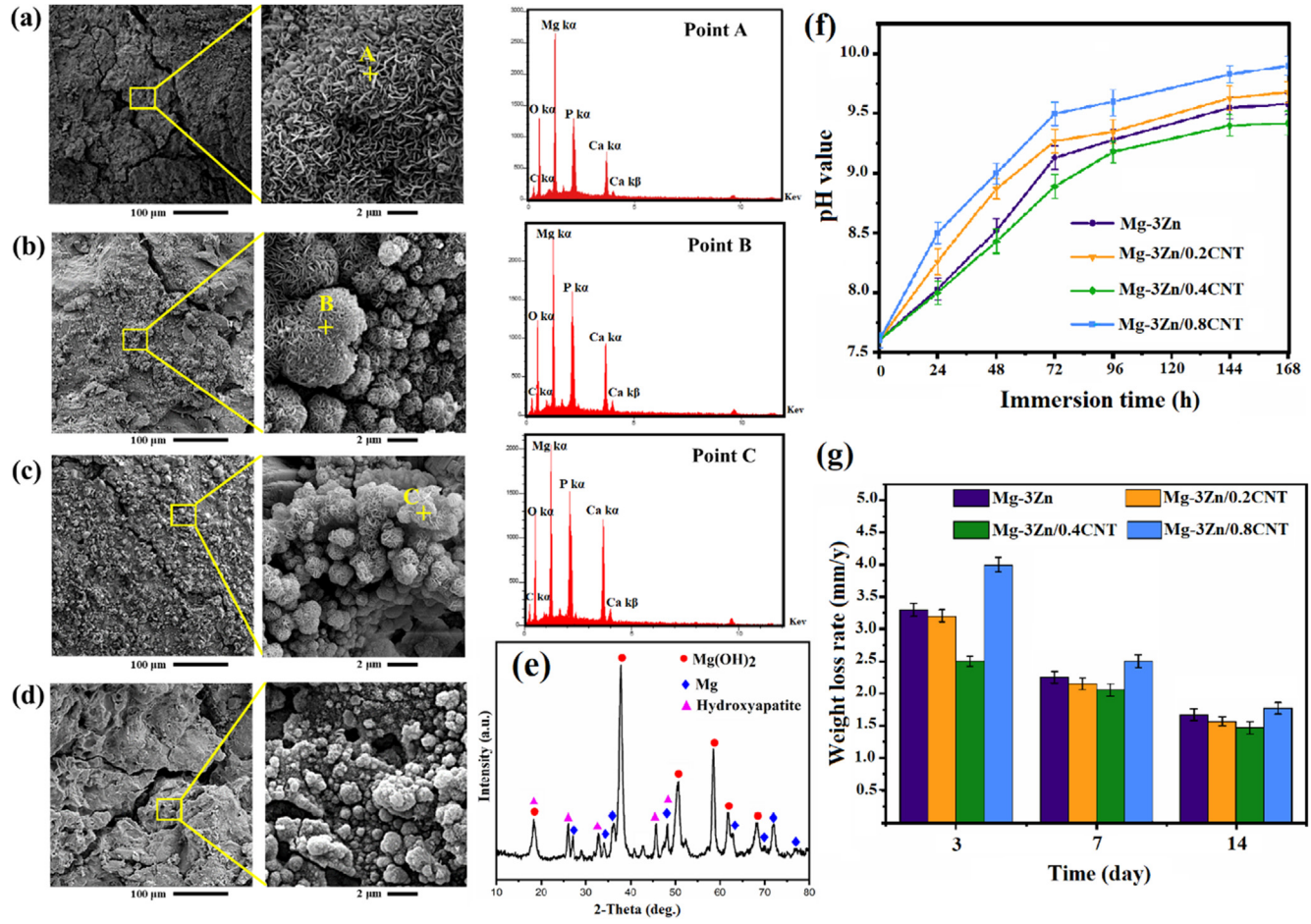


**Fig. 8.** SEM photomicrographs and EDX analysis of (a) Mg-3Zn, (b) Mg-3Zn/0.2fCNTs, (c) Mg-3Zn/0.4fCNTs and (d) Mg-3Zn/0.8fCNTs nanocomposites after 7 days of immersion in SBF solution at 37 °C, (e) XRD pattern of Mg-3Zn/0.4fCNTs immersed in SBF for 7 days, (f) pH values and (g) Weight loss rate of Mg-3Zn/xfCNTs (x = 0, 0.2, 0.4 and 0.8 wt%) nanocomposites after immersion in SBF solution for different time.

between the HA crystals, which can help in filling the empty sites in the matrix structure, thereby increasing corrosion protection [6]. The XRD pattern of the Mg-3Zn/0.4fCNTs after 7 days of immersion in SBF is presented in Fig. 8e. The results clearly depicted that the corrosion products were $Mg(OH)_2$ and HA [52].

Fig. 8f compares the pH alterations of the Mg-3Zn matrix and Mg-3Zn/fCNTs composites after immersion in SBF for 7 days. The pH of the Mg-3Zn increased gradually with immersion time and fCNTs content. During the initial immersion time, Mg-3Zn/fCNTs is in good contact with the SBF solution and thus susceptible to be attacked by the SBF environment, and resulting in a gradual rise in pH. After extending immersion time, Mg-3Zn/fCNTs is covered by corrosion product mainly composed of HA and $Mg(OH)_2$, indicating that it less significantly corroded, and pH values remain stable at 9.5.

The corrosion rate (CR) of the sintered samples of Mg-3Zn and Mg-3Zn/xfCNTs composites was evaluated by weight loss, as shown in Fig. 8g. In the case of the CR for the Mg-3Zn, Mg-3Zn/0.2fCNTs, Mg-3Zn/0.4fCNTs and Mg-3Zn/0.8fCNTs composites after 3 days of immersion, the weight-loss tests revealed 3.56, 3.13, and 2.74 and 3.84 mm/y, respectively. It can be seen that the CR from weight-loss investigations showed a high escalation in CR in the Mg-3Zn/0.8fCNTs as compared to the Mg-3Zn, and Mg-3Zn/0.4fCNTs. Recent researches on the corrosion inhibition capacity of fCNTs implied that fCNTs with $sp^2$ hybrid carbon atoms bonds were impermeable to gas molecules and provided an atomic-scale barrier through which not even helium gas could pass [40]. Another feature that decreases the CR of Mg-3Zn/0.4fCNT is grain refinement of Mg matrices via the addition of uniformly dispersed fCNTs [5,20].

Fig. 9a shows potentiodynamic polarization curves as a function of fCNTs concentration. The kinetic parameters are listed in Table 3. Even though the composite containing 0.4 wt% fCNTs has its corrosion potential (-1.405 $V_{SCE}$) slightly shifted toward the nobler-side potential (of about 0.012 $V_{SCE}$) when compared with the Mg-3Zn base alloy, the corresponding current density (96 $\mu A.cm^{-2}$) is reduced as compared to the Mg-3Zn alloy matrix (124.6 $\mu A.cm^{-2}$ and $-1.417$ $V_{SCE}$). In comparison to the base alloy and the composite with 0.2 wt% fCNTs (109.9 $\mu A.cm^{-2}$) and 0.8 wt% fCNTs (134.7 $\mu A.cm^{-2}$), the addition of 0.4 wt% fCNT srevealed excellent corrosion resistance. This indicates a good correlation between the results from immersion test and potentiodynamic polarization measurements. In comparison to previous researches [17,53,54], the higher corrosion rate in the composites was attributed to the high potential of the galvanic cells formed between the Mg matrix and the fCNTs reinforcement.

For additional confirmation of the polarization consequence, the EIS test for the Mg-3Zn/fCNTs composite in the SBF was conducted. Higher fCNTs content in the Mg-3Zn/fCNTs composite increases the dimensions of the capacitive loops up to 0.4 wt% fCNTs, indicating that fCNTs addition improved the corrosion resistance. The electrical elements described in the circuits inserted in Table 4 were used to fit the experimental data, where $R_s$ was the electrolyte resistance between the working and reference elec-

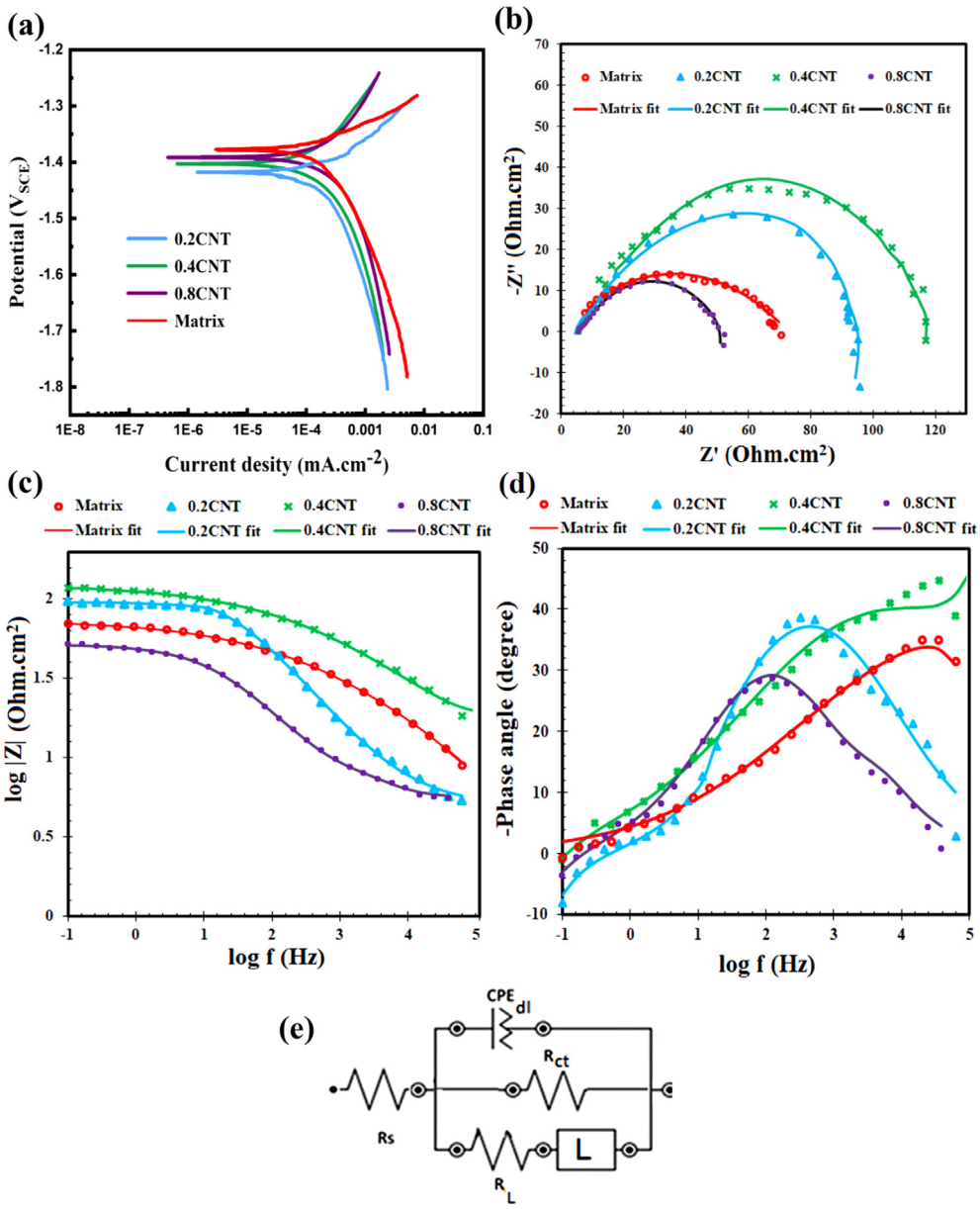


**Fig. 9.** (a) Potentiodynamic polarization curves and (b) Nyquist plots of Mg-3Zn/xfCNTs (x = 0, 0.2, 0.4, and 0.8 wt% fCNTs) composites, (c) Bode plot, (d) Bode phase angle plot and (e) equivalent circuit used to model the results of composites.

**Table 3**
Electrochemical parameters of samples in SBF attained from the polarization test of Mg-3Zn/fCNTs nanocomposites.

| Samples | $\beta_a$ ($v.dec^{-1}$) | $-\beta_c$ ($v.dec^{-1}$) | $E_{corr}$ SCE ($V_{SCE}$) | $i_{corr}$ ($\mu A.cm^{-2}$) | Corrosion rate (CR) (mmpy) |
|---|---|---|---|---|---|
| Mg-3Zn | 73.45 | 150.71 | −1.417 | 124.6 | 3.56 |
| Mg-3Zn/0.2fCNTs | 45.906 | 130.786 | −1.388 | 109.9 | 3.13 |
| Mg-3Zn/0.4fCNTs | 116.723 | 113.903 | −1.405 | 96 | 2.74 |
| Mg-3Zn/0.8fCNTs | 112.596 | 109.411 | −1.399 | 134.7 | 3.84 |

trodes, $R_{ct}$ was the charge transfer resistance, and $CPE_{dl}$ was the electric double-layer capacitance of the passive film. According to the fitting results, Mg-3Zn/0.4fCNTs has a higher $R_{ct}$ value (116.3 $\Omega.cm^2$) than Mg-3Zn (65.5 $\Omega.cm^2$), Mg-3Zn/0.2fCNTs (87.98 $\Omega.cm^2$) and Mg-3Zn/0.8fCNTs (47.58 $\Omega.cm^2$), which agrees well with the polarization results. Mg-3Zn/CNT nanocomposites, particularly Mg-3Zn/0.2fCNTs and Mg-3Zn/0.4fCNTs composites, demonstrated higher impedance and phase angles than Mg-3Zn alloy matrix in the middle and low-frequency ranges. This suggested that the addition of fCNTs increases the probability of corrosion. These findings revealed that adding more fCNTs (0.8 wt%) accelerated the degradation of Mg-3Zn, while no reversed effect was observed when less amount of fCNTs was encapsulated [35].

### 3.4. Biological properties

Since biomaterials are inserted into the body, successful integration of the implant with the body is dependent on tissue inte-

**Table 4**
Fitting results of equivalent circuit elements.

| Samples | $R_s$ (ohm.cm$^2$) | $R_{ct}$ (ohm.cm$^2$) | n | $CPE_{dl}$ (S.sec$^n$/cm$^2$) | $R_L$ (ohm.cm$^2$) | L (Henri.cm$^2$) |
|---|---|---|---|---|---|---|
| Mg-3Zn | 6.28 | 65.5 | 0.63 | $6.33 \times 10^{-4}$ | 0.94 | 682.2 |
| Mg-3Zn/0.2fCNTs | 5.25 | 87.98 | 0.72 | $1.53 \times 10^{-4}$ | 2.88 | 1006 |
| Mg-3Zn/0.4fCNTs | 4.01 | 116.3 | 0.93 | $5.63 \times 10^{-4}$ | 2.09 | 197 |
| Mg-3Zn/0.8fCNTs | 5.5 | 47.58 | 0.63 | $9.62 \times 10^{-4}$ | 0.67 | 828.4 |

gration via cell adhesion to the implant surface and later adsorption of specific proteins on the surface of the implant, which will facilitate cell attachment and biological reactions [40,42]. In general, osteoblast cells first bind to the implant surface and then deposit crystalline salts on the collagen matrix, resulting in mineralization and bone formation. As a result, osteoblast adhesion to the implant surface is critical for their proliferation and growth and further formation of mineral products.

It was reported [36] that the hydrophilicity of composites has a significant influence on their cell attachment and protein adsorption. Water contact angles were measured on samples containing different amounts of fCNTs to identify their hydrophilic characteristic, as shown in Fig. 10a. The water contact angle of Mg-3Zn was 97.7 ± 1.7°, which was expected due to its hydrophobic nature. With the addition of fCNTs, the hydrophilic property of Mg-3Zn was greatly improved [36]. Mg-3Zn/0.2fCNTs, Mg-3Zn/0.4fCNTs, and Mg-3Zn/0.8fCNTs had water contact angles of 86 ± 1.7, 73.8 ± 4.1 and 45.4 ± 3°, respectively. These findings could be explained by the hydrophilic property of fCNTs, which have a large number of oxygenated functional groups. Incorporating a higher content of fCNTs (>0.8 wt%) to Mg-3Zn alloy matrix can induce large agglomerations because of stacking of CNTs, resulting in more hydrophilic surfaces causes galvanic and crevice attacks in the SBF solution. During the anodic reaction, the hydrophilicity of the nanocomposites increases the release of electrons in the SBF immersion test [31]. Thus the corrosion resistance of composites decreases as hydrophilicity of the nanocomposites increases. Fluorescence images were used to evaluate MG-63 cell morphologies in extracts of Mg-3Zn/fCNTs composites in this study, and the results are shown in Fig. 10b. Mg-3Zn and Mg-3Zn/0.4fCNTs extracts supported cell growth and cell morphology was well defined after 24 h. The cells in extracts of Mg-3Zn/0.2fCNTs and Mg-3Zn/0.4fCNTs composites showed no noticeable difference in density and morphology, implying that the incorporation of fCNTs into Mg-3Zn had no detrimental effect on cell density and morphology when compared to Mg-3Zn, whereas incorporation of 0.8 wt% fCNTs had the opposite effect on cell viability [35]. SEM images of osteoblast cells (MG-63) on Mg-3Zn/fCNTs composites after 3 days of culture is shown in Fig. 10c. The extended and flattened morphology of cells on Mg-3Zn alloy and Mg-3Zn/0.4fCNTs composite suggests that Mg-3Zn/fCNTs composite is non-toxic and has good cytocompatibility [55]. The osteoblasts decrease significantly and have a relatively round morphology on the Mg-3Zn/0.8fCNTs composite (Fig. 10c), implying that composites with high fCNTs content have some negative effects on osteoblast attachment, spreading, and proliferation [55]. Moreover, the MG-63 cell proliferation in extracts of Mg-3Zn/fCNTs nanocomposites was evaluated by MTT assay, which reflected cell viability according to Ref. [35] as shown in Fig. 11a. With the increase of culture time, it was clear that all of the extracts escalated cell proliferation. Mg-3Zn/0.2fCNTs and Mg-3Zn/0.4fCNTs composites had a stimulatory effect on cell viability compared to the control group while further addition of fCNTs to 0.8 wt% had a more significant inhibitory action with the prolonged incubation. After 3 days of incuba-

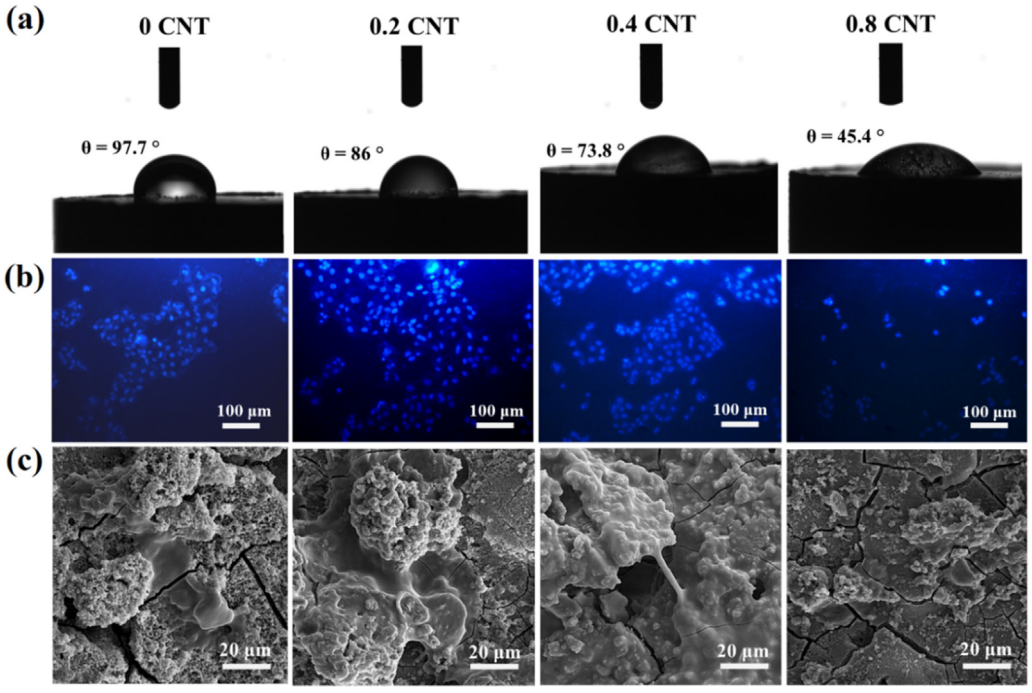


**Fig. 10.** (a) Images of water contact angle, (b) Fluorescent DAPI staining of MG-63 cells grown after 24 h, and (c) SEM images of the morphology and adhesion of these cells for 3 days on Mg-3Zn alloy matrix, Mg-3Zn/0.2fCNTs, Mg-3Zn/0.4fCNTs and Mg-3Zn/0.8fCNTs nanocomposites.

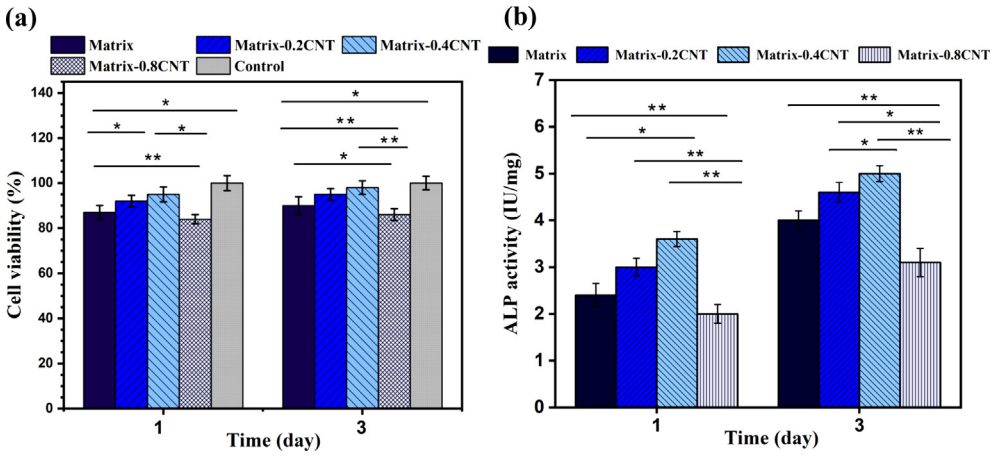


**Fig. 11.** (a) cell viability and (b) ALP activity of MG-63 cells cultured for various times on Mg-3Zn/xfCNTs (x = 0, 0.2, 0.4 and 0.8 wt% fCNTs) nanocomposites. (*p < 0.05 and **p < 0.01).

tion, cell viability for Mg-3Zn, Mg-3Zn/0.2fCNTs, Mg-3Zn/0.4fCNTs, and Mg-3Zn/0.8fCNTs was 90%, 95 %, 98 % and 86 %, respectively, which was much higher than 75 %, a criterion of good cytocompatibility [56]. The higher degradation rates caused by more serious galvanic corrosion could explain the increased toxicity with increased fCNTs content [35]. On the one hand, when compared to Mg-3Zn, the accelerated degradation would eventually result in more Mg ions being released, which has been shown to inhibit cell viability [57]. On the one hand, the accelerated degradation, resulted in a rapid increase in local pH, which may restrict cell viability [23,58–60]. As for the long-term degradation process of the composite, degradation products would gradually cover the matrix as time passed. To some extent, this inevitably hindered the infestation of corrosive medium. As a result, the degradation rate, as well as the pH, would remain stable. Cell viability enhanced steadily with increasing in vitro culture time, indicating improved cytocompatibility of the Mg-3Zn/fCNTs composites after long-term degradation. Besides, the metabolic process in the human body may decrease the toxicity induced by the released ions and boost pH. As a consequence, the cytocompatibility of the composites would improve during the long-term degradation process [35].

Fig. 11b shows the ALP activities of MG-63 cells after 1 and 3 days of cultivation on Mg-3Zn and Mg-3Zn/fCNTs composites. ALP was an initial differentiation marker that was involved in the formation of bone matrix and mineralization [7,55]. The ALP activity of Mg-3Zn/fCNTs nanocomposite is greater than that of the Mg-3Zn alloy matrix. All across the experiment period. On 1 and 3 days, Mg-3Zn/0.4fCNTs composite has a relatively higher ALP function than Mg-3Zn/0.2fCNTs composite and Mg-3Zn/0.8fCNTs composite has the minimum ALP activity. ALP expression suggests that the Mg-3Zn/fCNTs composites with lower fCNTs content benefit osteoblastic differentiation. The ALP activity of all Mg-3Zn/fCNTs composites is observed to be incubation time-dependent, with cell differentiation in the Mg-3Zn/fCNTs composite extracts increasing as the incubation time increases. The fact that Mg-3Zn/fCNTs composites with lower concentrations of fCNTs extracts have higher ALP activity suggests that they can promote cell differentiation in this study.

## 4. Conclusions

High strength Mg-3Zn/xfCNTs (x = 0, 0.2, 0.4 and 0.8 wt% fCNTs) nanocomposites were developed by semi-powder metallurgy integrated with sintering and extrusion process. The hardness, UCS and strain to failure of the Mg-3Zn/0.4fCNTs nanocomposite reached 74 ± 2.5 HV, 390 ± 15 MPa and 15.7 ± 1.5 %, respectively with a great improvement than that of the Mg-3Zn matrix without fCNTs. As a result, the semi-powder metallurgy and extrusion process have been proven to be an efficient and feasible method to fabricate high strength Mg-3Zn/fCNTs composites. The load-transfer mechanism is primarily responsible for the simultaneous strengthening contributions. The presence of CNT with functional groups in Mg-3Zn/fCNTs composites increases the nucleation sites, growth of hydroxyapatite crystals, and formation of bridges between hydroxyapatite structures. The Mg-3Zn/fCNTs composite could also significantly improve corrosion resistance over a relatively long period of time; however, corrosion resistance of the Mg-3Zn matrix was reduced if a high amount of fCNTs was used. More crucially, the structural properties of the Mg-3Zn/fCNTs composites endowed the material good biocompatibility and boosted the osteoblast cells (MG-63) viability when compared to Mg-3Zn alloy matrix without fCNTs. Combined with their superior mechanical characteristics, the Mg-3Zn/0.4fCNTs composites are greatly promising as a bone-implant material for bone tissue regeneration and replacement.

## Data Availability Statement

All the relevant data used in the study have been provided in the form of figures and tables in the published article, and all data provided in the present manuscript are available to whom it may concern.

## Declaration of Competing Interest

The authors declare that they have no known competing financial interests or personal relationships that could have appeared to influence the work reported in this paper.

## Appendix A. Supplementary material

Supplementary data to this article can be found online at https://doi.org/10.1016/j.matdes.2021.110354.

## References

[1] F. Chai, D. Zhang, W. Zhang, Y. Li, Microstructure evolution during high strain rate tensile deformation of a fine-grained AZ91 magnesium alloy, Mater. Sci. Eng. A. 590 (2014) 80–87.
[2] C.D. Li, X.J. Wang, W.Q. Liu, H.L. Shi, C. Ding, X.S. Hu, M.Y. Zheng, K. Wu, Effect of solidification on microstructures and mechanical properties of carbon

nanotubes reinforced magnesium matrix composite, Mater. Des. 58 (2014) 204–208.
[3] M. Rashad, F. Pan, A. Tang, Y. Lu, M. Asif, S. Hussain, J. She, J. Gou, J. Mao, Effect of graphene nanoplatelets (GNPs) addition on strength and ductility of magnesium-titanium alloys, J. Magnes. Alloy. 1 (3) (2013) 242–248.
[4] M.R. Barnett, A. Ghaderi, J. Quinta da Fonseca, J.D. Robson, Influence of orientation on twin nucleation and growth at low strains in a magnesium alloy, Acta Mater. 80 (2014) 380–391.
[5] J. Hou, W. Du, G. Parande, M. Gupta, S. Li, Significantly enhancing the strength + ductility combination of Mg-9Al alloy using multi-walled carbon nanotubes, J. Alloys Compd. 790 (2019) 974–982.
[6] D. Khazeni, M. Saremi, R. Soltani, Development of HA-CNTs composite coating on AZ31 magnesium alloy by cathodic electrodeposition. Part 1: microstructural and mechanical characterization, Ceram. Int. 45 (9) (2019) 11174–11185.
[7] C. Shuai, B. Wang, S. Bin, S. Peng, C. Gao, Interfacial strengthening by reduced graphene oxide coated with MgO in biodegradable Mg composites, Mater. Des. 191 (2020) 108612, https://doi.org/10.1016/j.matdes.2020.108612.
[8] Z. Li, L. Chen, X. Zhang, G. Zhao, C. Zhang, Strengthening mechanism and anisotropy of mechanical properties of Si3N4p/Al-Mg-Si composites fabricated by sintering and extrusion, Mater. Des. 210 (2021) 110111.
[9] F. Sun, C. Shi, K.Y. Rhee, N. Zhao, In situ synthesis of CNTs in Mg powder at low temperature for fabricating reinforced Mg composites, J. Alloys Compd. 551 (2013) 496–501.
[10] S. Dasilva, A. Jimenez-Suarez, E. Rodríguez, S.G. Prolongo, Quality assessment and structural health monitoring of CNT reinforced CFRP and Ti6Al4V multi-material joints, Mater. Des. 210 (2021) 110118.
[11] M.-F. Yu, B.S. Files, S. Arepalli, R.S. Ruoff, Tensile loading of ropes of single wall carbon nanotubes and their mechanical properties, Phys. Rev. Lett. 84 (2000) 5552.
[12] M. Paramsothy, J. Chan, R. Kwok, M. Gupta, Addition of CNTs to enhance tensile/compressive response of magnesium alloy ZK60A, Compos. Part A Appl. Sci. Manuf. 42 (2) (2011) 180–188.
[13] Y. Ding, J. Xu, J. Hu, Q. Gao, X. Guo, R. Zhang, L. An, High performance carbon nanotube-reinforced magnesium nanocomposite, Mater. Sci. Eng. A. 771 (2020) 138575.
[14] A.V. Radhamani, H.C. Lau, S. Ramakrishna, CNT-reinforced metal and steel nanocomposites: a comprehensive assessment of progress and future directions, Compos. Part A Appl. Sci. Manuf. 114 (2018) 170–187.
[15] K.K.H. Wong, M. Zinke-Allmang, J.L. Hutter, S. Hrapovic, J.H.T. Luong, W. Wan, The effect of carbon nanotube aspect ratio and loading on the elastic modulus of electrospun poly (vinyl alcohol)-carbon nanotube hybrid fibers, Carbon N. Y. 47 (11) (2009) 2571–2578.
[16] H. Fukuda, K. Kondoh, J. Umeda, B. Fugetsu, Fabrication of magnesium based composites reinforced with carbon nanotubes having superior mechanical properties, Mater. Chem. Phys. 127 (3) (2011) 451–458.
[17] H. Mindivan, A. Efe, A.H. Kosatepe, E.S. Kayali, Fabrication and characterization of carbon nanotube reinforced magnesium matrix composites, Appl. Surf. Sci. 318 (2014) 234–243.
[18] J. Hou, W. Du, Z. Wang, S. Li, K.e. Liu, X. Du, Combination of enhanced thermal conductivity and strength of MWCNTs reinforced Mg-6Zn matrix composite, J. Alloys Compd. 838 (2020) 155573, https://doi.org/10.1016/j.jallcom.2020.155573.
[19] X.-S. Zeng, Y. Liu, Q.-y. Huang, G. Zeng, G.-H. Zhou, Effects of carbon nanotubes on the microstructure and mechanical properties of the wrought Mg–2.0 Zn alloy, Mater. Sci. Eng. A. 571 (2013) 150–154.
[20] Y. Huang, J. Li, L. Wan, X. Meng, Y. Xie, Strengthening and toughening mechanisms of CNTs/Mg-6Zn composites via friction stir processing, Mater. Sci. Eng. A. 732 (2018) 205–211.
[21] N. Darsono, M. Handayani, F.P. Lestari, A. Erryani, I. Putrayasa, Y.N. Thaha, Y.I. Sihaloho, H. Sutanto, Effect of multiwalled carbon nanotubes (MWCNTs) on the micro-hardness and corrosion behaviour Mg-Zn alloy prepared by powder metallurgy, in: Mater. Sci. Forum, Trans Tech Publ, 2020, pp. 115–122.
[22] T. Kokubo, H. Takadama, How useful is SBF in predicting in vivo bone bioactivity?, Biomaterials 27 (15) (2006) 2907–2915
[23] C. Shuai, B. Wang, Y. Yang, S. Peng, C. Gao, 3D honeycomb nanostructure-encapsulated magnesium alloys with superior corrosion resistance and mechanical properties, Compos. Part B Eng. 162 (2019) 611–620.
[24] S. Baradaran, E. Moghaddam, W.J. Basirun, M. Mehrali, M. Sookhakian, M. Hamdi, M.R.N. Moghaddam, Y. Alias, Mechanical properties and biomedical applications of a nanotube hydroxyapatite-reduced graphene oxide composite, Carbon N. Y. 69 (2014) 32–45.
[25] Q.-H. Yuan, X.-S. Zeng, Y. Liu, L. Luo, J.-B. Wu, Y.-C. Wang, G.-H. Zhou, Microstructure and mechanical properties of AZ91 alloy reinforced by carbon nanotubes coated with MgO, Carbon N. Y. 96 (2016) 843–855.
[26] C. Shuai, T. Liu, C. Gao, P. Feng, T. Xiao, K. Yu, S. Peng, Mechanical and structural characterization of diopside scaffolds reinforced with graphene, J. Alloys Compd. 655 (2016) 86–92.
[27] M. Shahin, K. Munir, C. Wen, Y. Li, Magnesium-based composites reinforced with graphene nanoplatelets as biodegradable implant materials, J. Alloys Compd. 828 (2020) 154461.
[28] H. Kabir, K. Munir, C. Wen, Y. Li, Recent research and progress of biodegradable zinc alloys and composites for biomedical applications: biomechanical and biocorrosion perspectives, Bioact. Mater. 6 (2021) 836–879.
[29] S. Ramezanzade, G.R. Ebrahimi, M.T. Parizi, H.R. Ezatpour, Synergetic effect of GNPs and MgOs on the mechanical properties of Mg–Sr–Ca alloy, Mater. Sci. Eng. A. 761 (2019) 138025.
[30] S. Zhang, X. Zhang, C. Zhao, J. Li, Y. Song, C. Xie, H. Tao, Y. Zhang, Y. He, Y. Jiang, Y. Bian, Research on an Mg–Zn alloy as a degradable biomaterial, Acta Biomater. 6 (2010) 626–640.
[31] M. Shahin, C. Wen, K. Munir, Y. Li, Mechanical and corrosion properties of graphene nanoplatelet–reinforced Mg–Zr and Mg–Zr–Zn matrix nanocomposites for biomedical applications, J. Magnesium Alloys (2021), https://doi.org/10.1016/j.jma.2021.05.011.
[32] C.S. Goh, J. Wei, L.C. Lee, M. Gupta, Ductility improvement and fatigue studies in Mg-CNT nanocomposites, Compos. Sci. Technol. 68 (6) (2008) 1432–1439.
[33] K.S. Tun, P. Jayaramanavar, Q.B. Nguyen, J. Chan, R. Kwok, M. Gupta, Investigation into tensile and compressive responses of Mg–ZnO composites, Mater. Sci. Technol. 28 (5) (2012) 582–588.
[34] Q.B. Nguyen, M. Gupta, Increasing significantly the failure strain and work of fracture of solidification processed AZ31B using nano-Al2O3 particulates, J. Alloys Compd. 459 (1-2) (2008) 244–250.
[35] C. Shuai, S. Li, G. Wang, Y. Yang, S. Peng, C. Gao, Strong corrosion induced by carbon nanotubes to accelerate Fe biodegradation, Mater. Sci. Eng. C. 104 (2019) 109935.
[36] C. Shuai, Z. Zeng, Y. Yang, F. Qi, S. Peng, W. Yang, C. He, G. Wang, G. Qian, Graphene oxide assists polyvinylidene fluoride scaffold to reconstruct electrical microenvironment of bone tissue, Mater. Des. 190 (2020) 108564.
[37] K. Kondoh, H. Fukuda, J. Umeda, H. Imai, B. Fugetsu, M. Endo, Microstructural and mechanical analysis of carbon nanotube reinforced magnesium alloy powder composites, Mater. Sci. Eng. A. 527 (16-17) (2010) 4103–4108.
[38] G.Q. Han, J.H. Shen, X.X. Ye, B. Chen, H. Imai, K. Kondoh, W.B. Du, The influence of CNTs on the microstructure and ductility of CNT/Mg composites, Mater. Lett. 181 (2016) 300–304.
[39] Q. Li, A. Viereckl, C.A. Rottmair, R.F. Singer, Improved processing of carbon nanotube/magnesium alloy composites, Compos. Sci. Technol. 69 (7-8) (2009) 1193–1199.
[40] K.S. Munir, C. Wen, Y. Li, Carbon nanotubes and graphene as nanoreinforcements in metallic biomaterials: a review, Adv. Biosyst. 3 (3) (2019) 1800212, https://doi.org/10.1002/adbi.v3.310.1002/adbi.201800212.
[41] L.P. Zanello, B. Zhao, H. Hu, R.C. Haddon, Bone cell proliferation on carbon nanotubes, Nano Lett. 6 (3) (2006) 562–567.
[42] M. Shahin, K. Munir, C. Wen, Y. Li, Magnesium matrix nanocomposites for orthopedic applications: a review from mechanical, corrosion, and biological perspectives, Acta Biomater. 96 (2019) 1–19.
[43] A. Dubey, S. Jaiswal, S. Haldar, P. Roy, D. Lahiri, Mg-3Zn/HA biodegradable composites synthesized via spark plasma sintering for temporary orthopedic implants, J. Mater. Eng. Perform. 28 (9) (2019) 5702–5715.
[44] S. Jaiswal, R.M. Kumar, P. Gupta, M. Kumaraswamy, P. Roy, D. Lahiri, Mechanical, corrosion and biocompatibility behaviour of Mg-3Zn-HA biodegradable composites for orthopaedic fixture accessories, J. Mech. Behav. Biomed. Mater. 78 (2018) 442–454.
[45] M. Razzaghi, M. Kasiri-Asgarani, H.R. Bakhsheshi-Rad, H. Ghayour, In vitro degradation, antibacterial activity and cytotoxicity of Mg-3Zn-xAg nanocomposites synthesized by mechanical alloying for implant applications, J. Mater. Eng. Perform. 28 (3) (2019) 1441–1455.
[46] G.K. Meenashisundaram, M.H. Nai, A. Almajid, M. Gupta, Development of high performance Mg–TiO2 nanocomposites targeting for biomedical/structural applications, Mater. Des. 65 (2015) 104–114.
[47] F. Witte, N. Hort, C. Vogt, S. Cohen, K.U. Kainer, R. Willumeit, F. Feyerabend, Degradable biomaterials based on magnesium corrosion, Curr. Opin. Solid State Mater. Sci. 12 (5-6) (2008) 63–72.
[48] M.K. Habibi, M. Paramsothy, A.M.S. Hamouda, M. Gupta, Enhanced compressive response of hybrid Mg–CNT nano-composites, J. Mater. Sci. 46 (13) (2011) 4588–4597.
[49] A.K. Khanra, H.C. Jung, K.S. Hong, K.S. Shin, Comparative property study on extruded Mg–HAP and ZM61–HAP composites, Mater. Sci. Eng. A. 527 (23) (2010) 6283–6288.
[50] S. Abazari, A. Shamsipur, H.R. Bakhsheshi-Rad, S. Ramakrishna, F. Berto, Graphene family nanomaterial reinforced magnesium-based matrix composites for biomedical application: a comprehensive review, Metals (Basel) 10 (8) (2020) 1002, https://doi.org/10.3390/met10081002.
[51] A.M. Kumar, S.F. Hassan, A.A. Sorour, M. Paramsothy, M. Gupta, Investigation on the controlled degradation and invitro mineralization of carbon nanotube reinforced AZ31 nanocomposite in simulated body fluid, Met. Mater. Int. 25 (1) (2019) 105–116.
[52] Z. Li, X. Gu, S. Lou, Y. Zheng, The development of binary Mg–Ca alloys for use as biodegradable materials within bone, Biomaterials 29 (10) (2008) 1329–1344.
[53] K. Funatsu, H. Fukuda, R. Takei, J. Umeda, K. Kondoh, Quantitative evaluation of initial galvanic corrosion behavior of CNTs reinforced Mg–Al alloy, Adv. Powder Technol. 24 (5) (2013) 833–837.
[54] N.N. Aung, W. Zhou, C.S. Goh, S.M.L. Nai, J. Wei, Effect of carbon nanotubes on corrosion of Mg–CNT composites, Corros. Sci. 52 (5) (2010) 1551–1553.
[55] H. Li, X. Song, B. Li, J. Kang, C. Liang, H. Wang, Z. Yu, Z. Qiao, Carbon nanotube-reinforced mesoporous hydroxyapatite composites with excellent mechanical and biological properties for bone replacement material application, Mater. Sci. Eng. C. 77 (2017) 1078–1087.
[56] C. Shuai, L. Liu, M. Zhao, P. Feng, Y. Yang, W. Guo, C. Gao, F. Yuan, Microstructure, biodegradation, antibacterial and mechanical properties of

ZK60-Cu alloys prepared by selective laser melting technique, J. Mater. Sci. Technol. 34 (10) (2018) 1944–1952.
[57] E. Zhang, H. Chen, F. Shen, Biocorrosion properties and blood and cell compatibility of pure iron as a biodegradable biomaterial, J. Mater. Sci. Mater. Med. 21 (7) (2010) 2151–2163.
[58] D. Zander, N.A. Zumdick, Influence of Ca and Zn on the microstructure and corrosion of biodegradable Mg–Ca–Zn alloys, Corros. Sci. 93 (2015) 222–233.
[59] L. Chen, Y. Sheng, H. Zhou, Z. Li, X. Wang, W. Li, Influence of a MAO+ PLGA coating on biocorrosion and stress corrosion cracking behavior of a magnesium alloy in a physiological environment, Corros. Sci. 148 (2019) 134–143.
[60] F. Lyu, J. Gao, N. Sun, R. Liu, X. Sun, X. Cao, L.i. Wang, W. Sun, Utilisation of propyl gallate as a novel selective collector for diaspore flotation, Miner. Eng. 131 (2019) 66–72.